LiDAR Remote Sensing Data Collection:
Bridge Creek, Oregon

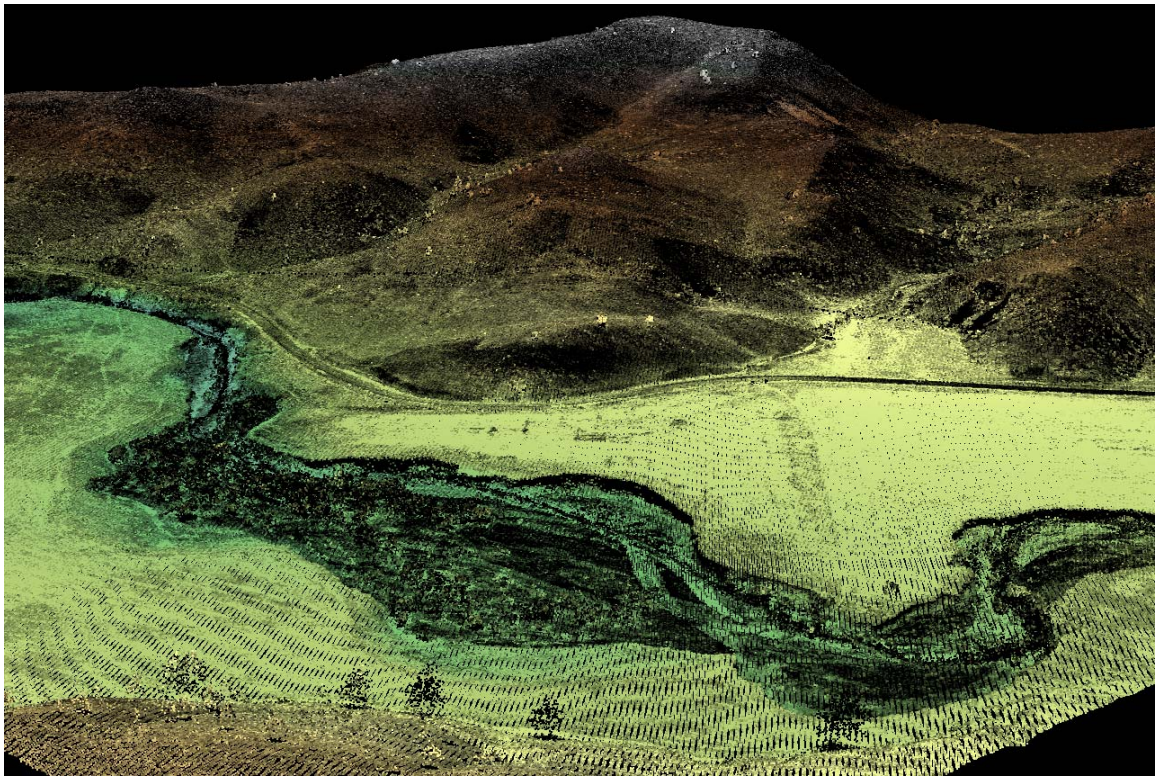

Submitted to:

Michael Pollock
Northwest Fisheries Science Center
2725 Montlake Blvd. E.
Seattle, Washington 98112

Submitted by:

Russ Faux
230 SW Third Street, Suite 202
Corvallis, Oregon 97333
971-223-5096

January, 2006

Table of Contents

Figures

Tables

Light Detection and Ranging (LiDAR)

Overview

Watershed Sciences, Inc. (WS) collected Light Detection and Ranging (LiDAR) data for the Northwest Fisheries Science Center on September 27, 2005. The survey area is located northwest of Mitchell, Oregon, and covers the lower ~ 16 RM of Bridge Creek from just above the Nelson Creek confluence to the mouth at the John Day River. The study area encompasses ~30,523 acres.

Laser points were collected over the study area using an Optech ALTM 3100 LiDAR system set to acquire points at an average spacing of >7 points per square meter. The system also recorded individual return intensities (per laser return) that are used to create combined elevation models that display both elevation and surface reflectivity.

Two differential GPS units were deployed and used to process kinematic solutions to the onboard GPS and inertial measurement unit (IMU) using PosPAC v4.2. Points were computed per flight line using the REALM Survey Suite v3.5.2. Microstation V8 and TerraScan were used to import the points into bins, remove pits and birds, and compute the bare earth model. TerraModeler was then used to create TINs and output ARCINFO ASCII lattice models, which were then imported into ArcMap to render one-meter mosaics of all returns and ground models.

Figure 1. Full extent of Study Area covering ~30,523 acres; 1-meter bare earth mosaic and hillshade shown with 10 meter DEM hillshade in background.

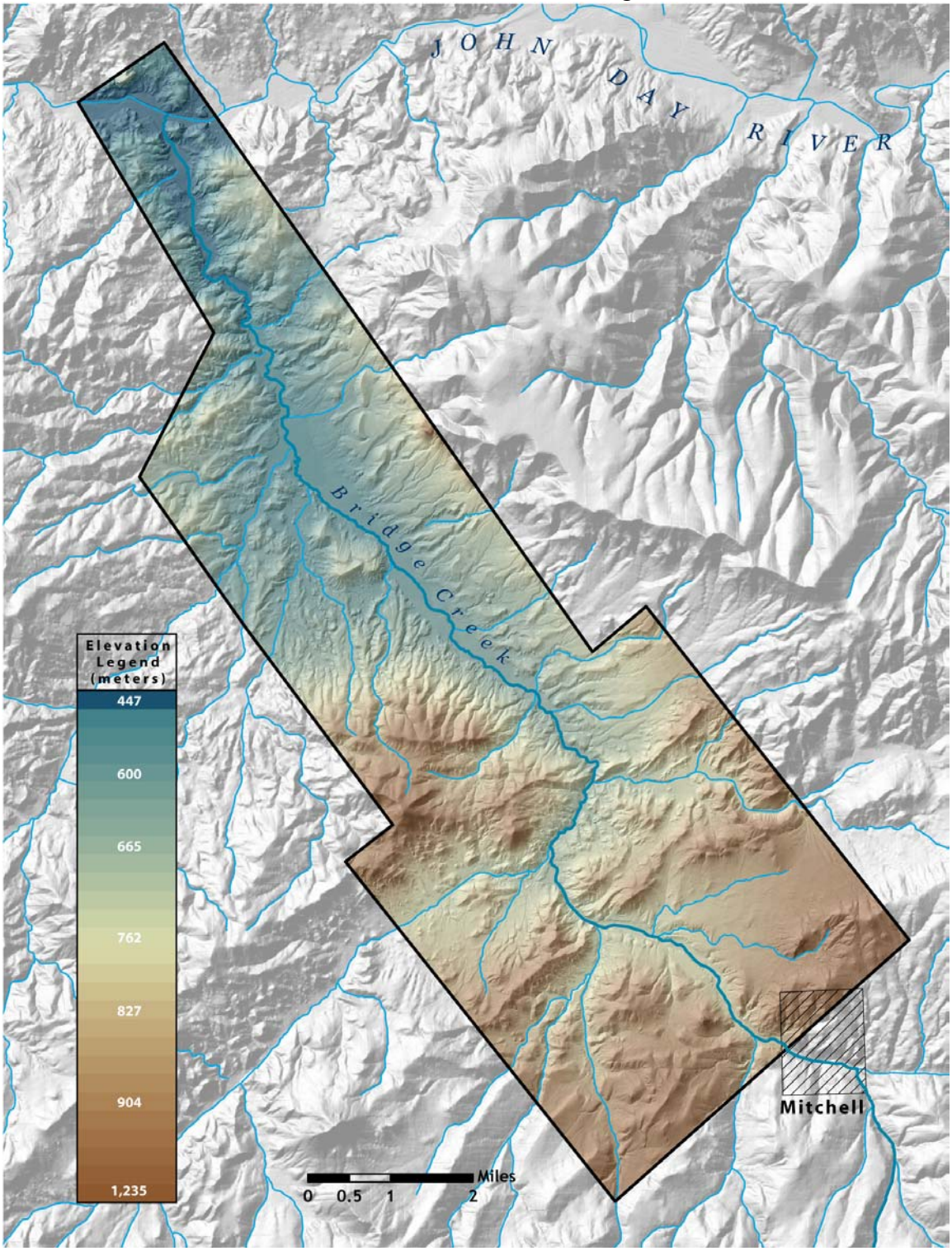

Laser point absolute accuracy is largely a function of internal consistency and laser noise:

- **Absolute Accuracy**: This is the comparison of laser points to real time kinematic (RTK) ground level survey data. A total of 1,027 RTK GPS measurements were compared to ground laser points collected for comparison with the LiDAR point data. The standard deviation is 0.041 meters and the deviation RMSE is 0.061 meters, with a median (50^{th} percentile) absolute deviation of 0.048 meters and a 95^{th} percentile of 0.109 meters.

- **Internal Consistency**: Internal consistency refers to the ability to place a laser point in the same location over multiple flight lines, GPS conditions and aircraft attitudes. The data were analyzed for internal consistency between opposing and orthogonal flight lines and passed divergence test requirements of less than 0.15 meters per any one overlapping flight line.

- **Laser Noise**: For any given target, laser noise is the breadth of the data cloud per laser return (i.e., last, first, etc.). Lower intensity surfaces (roads, rooftops, still/calm water) will experience higher laser noise. The laser noise range for this mission varies between 0.040 - 0.070 meters.

Technical Approach

Data Collection

Our LiDAR system is mounted in the belly of a Cessna Caravan 208. Quality control (QC) pre-mission flights were performed based on manufacturer's specifications prior to the survey. The QC flight was conducted at the Ashland Airport using known surveyed control points. The positional accuracy of the LiDAR (x, y, z) returns are checked against these known locations to verify the calibration and to report base accuracy.

The Optech 3100 system was set to a 71kHz laser repetition rate and flown at 1,100 meters above ground level (AGL), capturing a 30^{o} scan width (15^{o} from NADIR). These settings yielded points with an average spacing of >7 per square meter, with an average spot spacing of 37cm. The entire area was surveyed with opposing flight line overlap of 50% to reduce laser shadowing and increase surface laser painting. The system allows up to four range measurements per pulse, and all were processed for the output datasets. The data stream from the IMU was stored independently during the flight, and was differentially corrected and integrated with LiDAR pulse data during post processing. Throughout the survey, two dual frequency DGPS base stations located centrally in the study area recorded fast static (1 Hz) data. The base stations' coordinates were verified and corrected using the Online User Positioning System (OPUS), which is administered by the National Geodetic Survey (NGS).

Table 1. Base Station Surveyed Coordinates

Point ID	***NAD83NAVD88***		
	Latitude (North)	***Longitude (West)***	***Ellipsoid Height (m)***
BRIDGE 1 (OPUS Corrected)	44°37'50.21604"	120°13'03.22423"	636.124
BRIDGE 2 (OPUS corrected)	44°39'00.28010"	120°16'02.27024"	616.350

Data Acquisition Specifications

LiDAR Data Acquisition Feature	***Specification***
Laser Pulse Repetition Frequency	71 kHz
Laser Pulse Repetition Rate	≤71,000 pulses/sec
Operating Altitude	1,100 m AGL
Scan Frequency	37 Hz
Scan Angle	30° (+15° to -15° from Nadir)
Scan Pattern	Sawtooth
Laser Footprint Diameter on Ground (at 1,100 m AGL)	30-33 cm
Number of Returns Collected Per Laser Pulse	4
Multi-Swath Pulse Density	≥7 pulse/m^2
Intensity Range	8 bits
Minimum Resolvable Distance Between Returns	2.5 cm
Swath Width	714.8 m
Adjacent Swath Overlap (Side-Lap)	≥50%
Laser Spot Spacing (Cross Track = Along Track)	Single Swath: ≤0.73 m (≥2 pts/m^2) Multi Swath: ≤0.36 m (≥7 pts/m^2)
Vertical RMSE of LiDAR Survey	0.061 m
Number of GPS Base Stations Used	2
Maximum Distance From Airborne to Ground GPS	15 km (9.3 miles)
GPS PDOP During Acquisition	≤3.5
GPS Satellite Constellation During Acquisition	≥6
RTK Quality Control Data Points Collected	1,027
RTK Data RMSE	≤2.0 cm

Figure 2. The Cessna Caravan 208 - A removable composite cargo pod provides housing for GPS equipment and the LiDAR system and other remote sensing equipment.

Flight Parameters

System:	Optech 3100
Flight AGL (m):	1,100 m
Flight Speed:	105 knots
Scan Width:	30^{o} (15^{o} from NADIR)
Scan Pulse Repetition Frequency (PRF):	71,000 pulses per second (71kHz)

A total of 1,027 quality control real-time kinematic (RTK) GPS data points were collected within the project area using a ground based DGPS station. Data collected were then compared to the processed LiDAR data to ensure accuracies across the project area.

Figure 3. GPS Monuments and Ground Survey Points. (A) Two OPUS corrected base stations were used to survey fast static (1 Hz) data during the LiDAR survey. (B) A total of 1,027 ground survey points (RTK) were collected throughout the study area. These RTK points were used to assess data quality and accuracy. The surface shown here is a mosaic of all return points, created from a highest hit model. Shown with hillshade and 10 meter DEM hillshade in background.

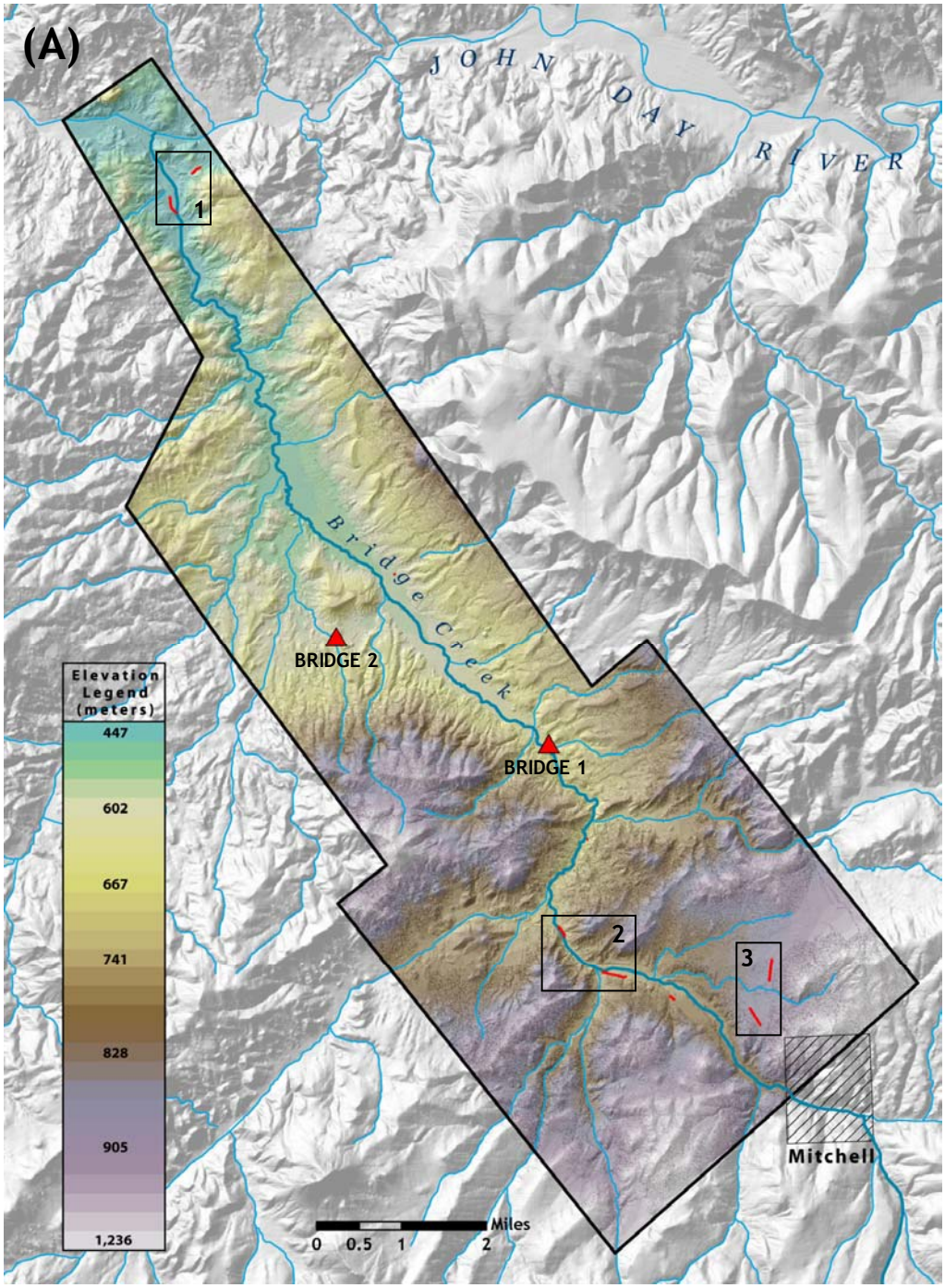

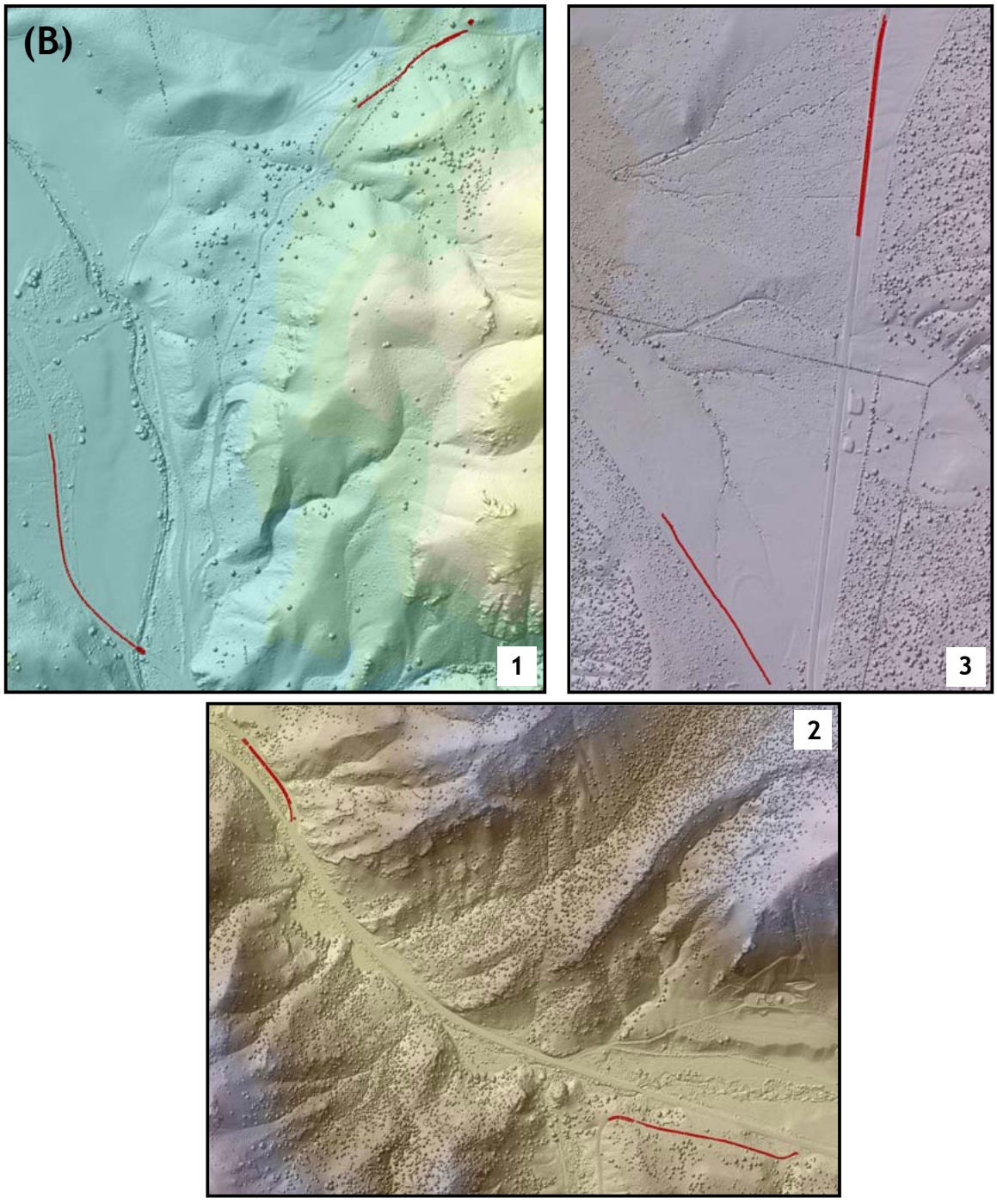
(B)
1
2
3

Data Processing

Coordinate System and Units

All data and imagery are developed as:

UTM zone 10, NAD83, NAVD88, Geoid03 S.I. Units

Laser point return coordinates were computed using the REALM software suite based on independent data from the LiDAR system (pulse time, scan angle), IMU (aircraft attitude), and aircraft position (differentially corrected and optimized using the multiple DGPS base stations data). The inertial measurement data were used to calculate the kinematic corrections for the aircraft trajectories using PosPAC v4.2. Flight lines and LiDAR data were reviewed to ensure complete coverage of the study area and positional accuracy of the laser points.

TerraScan Processing

To facilitate laser point processing, the first step is to create bins (polygons) that divide the data set into manageable sizes. The entire buffered study area was divided into 140 individual bins, approximately 1 km^2 each (see figure, below).

Figure 4. Processing Bins – 140 Total Bins; approximately 1 km x 1 km each. 1-meter bare earth mosaic and hillshade shown with 10 meter DEM hillshade in background.

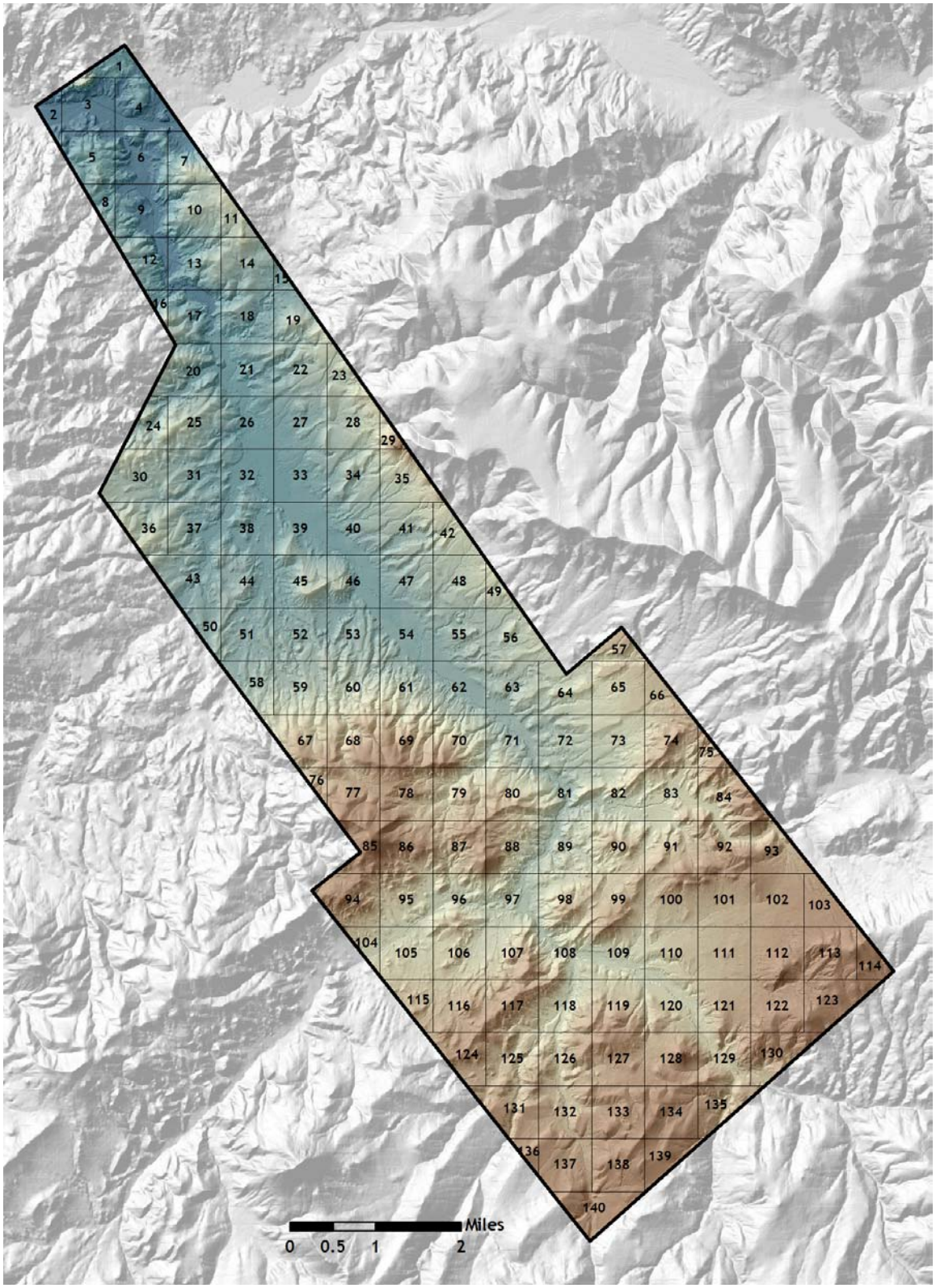

Laser point returns (first through fourth) are assigned an associated (x, y, z) coordinate, along with unique intensity values. The raw LiDAR points are filtered for noise, pits and birds by screening for absolute elevation limits, isolated points and height above ground. These data have passed initial screening and are deemed accurate.

No weeding or superfluous point removal was performed. The intent of a LiDAR survey is to accurately place points on targets, not remove points. If laser noise is low and internally consistent, aside from pits and birds, it is assumed that the remaining laser returns are from targets within the survey area.

The TerraScan software suite is designed specifically for developing a standard bare earth model to remove buildings, vegetation, and other features. The high point density and multiple returns result in uncomplicated identification of vegetated and obscured areas using first and last returns. The processing sequence begins by removing all points that are not "near" the earth based on evaluation of the multi-return layers.

The resulting bare earth (ground) model is visually inspected and additional ground modeling is performed in site specific areas (over a 50 meter radius) to improve ground detail. This is only done in areas with known ground modeling deficiencies, such as: bedrock outcrops, cliffs, deeply incised stream banks, and dense vegetation.

The vegetation surface model is developed using all (first through fourth) accurate laser returns, using a highest hit algorithm in surface creation. This results in a dataset comprised of the highest laser hits, i.e., rooftops and vegetation surfaces.

Using the difference between the vegetation surface model and the bare earth (ground) model, we have created a vegetation height ESRI GRID dataset. Null values in this dataset represent areas of insufficient information, such as on steep slopes where interpolation in the input GRIDs is not of sufficient resolution.

Statement of Accuracy

Table 2. Absolute Accuracy – Divergence between laser points and RTK survey points.

Standard Deviation:	0.041 m	5th Percentile:	0.004 m
RMSE:	0.061 m	25th Percentile:	0.023 m
n:	1,027	50th Percentile:	0.048 m
Minimum Δz:	-0.148	75th Percentile:	0.076 m
Maximum Δz:	0.062	95th Percentile:	0.109 m
Average Magnitude:	0.052 m		

Figure 5. Point Divergence Statistics
(A) Ground survey point deviation from laser points
(B) Absolute deviation from laser points, with percentile statistics

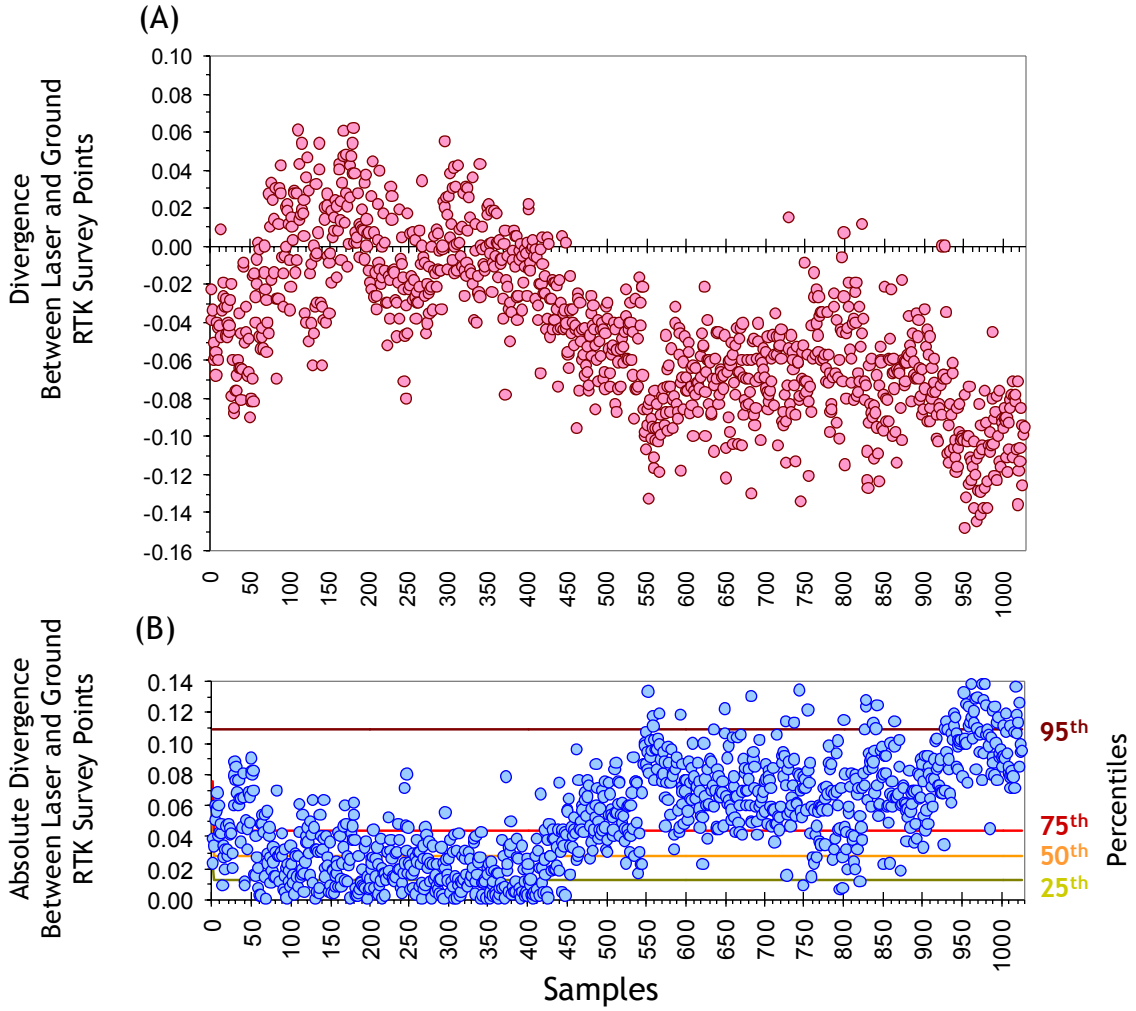

Table 3. LiDAR accuracy is a combination of several sources of error. These sources of error are cumulative. Some error sources that are biased and act in a patterned displacement can be resolved in post processing.

Type of Error	Source	Post Processing Solution	Effect
GPS (Static/Kinematic)	Long Base Lines	None	
	Poor Satellite Constellation	None	
	Poor Antenna Visibility	Reduce Visibility Mask	Slight
Internal Consistency	Poor System Calibration	Recalibration IMU and sensor offsets/settings	Large
	Inaccurate System	None	
Laser Noise	Poor Laser Timing	None	
	Poor Laser Reception	None	

Quality Assurance and Control

Quality assurance and control is built into the overall methodology. The data collection was monitored using the diagnostic features of the system during the flight. The precise navigation system and 50% side over-lap during acquisition is designed to eliminate missing coverage and ensure laser painting of multiple sides of surfaces. Over areas with significant topographic relief, additional lines were flown to ensure complete and consistent overlap. The quality of the GPS signal (or PDOP) is recorded throughout the flight and only PDOP values less than 3.5 are accepted.

All of the data are delivered on hard drive, along with this report.

Deliverables

Data Report

Points

- LAS: all returns per bin

Rasters

- **GEOTIFFs**
  GEOTIFFs of all returns (first through fourth and ground model points) elevations, shaded by intensity, per bin.

- **Bare_Earth_1m**
  Triangulated Model of Ground Points:
  1.0 meter resolution mosaic in ESRI GRID format

- **Veg_Surface_1m**
  All Returns Highest Hit Model of Vegetation Surface:
  1.0 meter resolution mosaic in ESRI GRID format

- **Veg_Height_1m**
  Vegetation Heights:
  (Derived from difference between highest hits and ground model)
  1.0 meter resolution mosaic in ESRI GRID format

  (Note: Null values in this dataset reflect insufficient information for an accurate calculation).

Selected Images

Figure 6. Map of bins 17-18, 20-21, showing Bridge Creek just below Lockwood Canyon. Vegetation grid derived from difference between all returns and bare ground surface, shown over all returns hillshade derived from 1-meter grid. Inset shows location within study area.

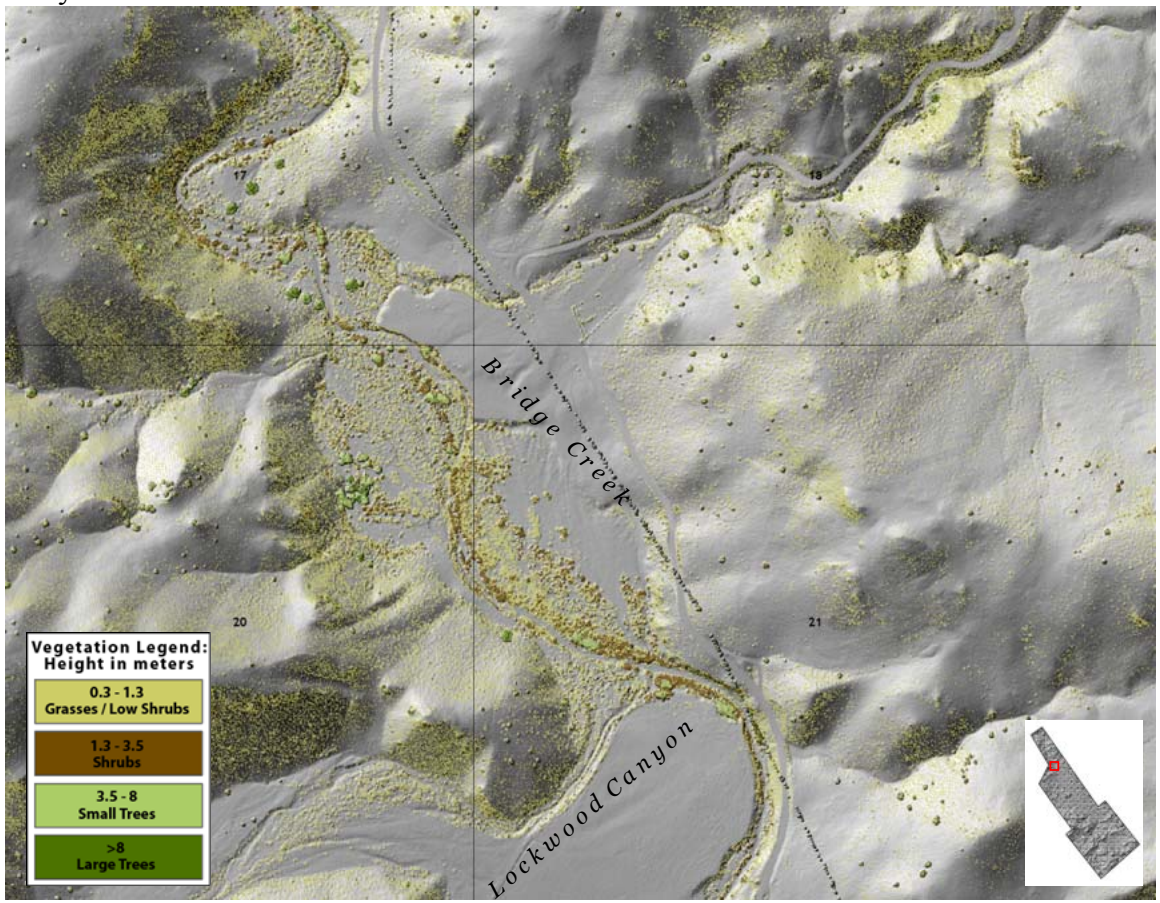

Figure 7. Map of bins 17-18, 20-21, showing Bridge Creek just below Lockwood Canyon. Bare ground hillshade, derived from 1-meter grid, showing morphology underneath vegetation.

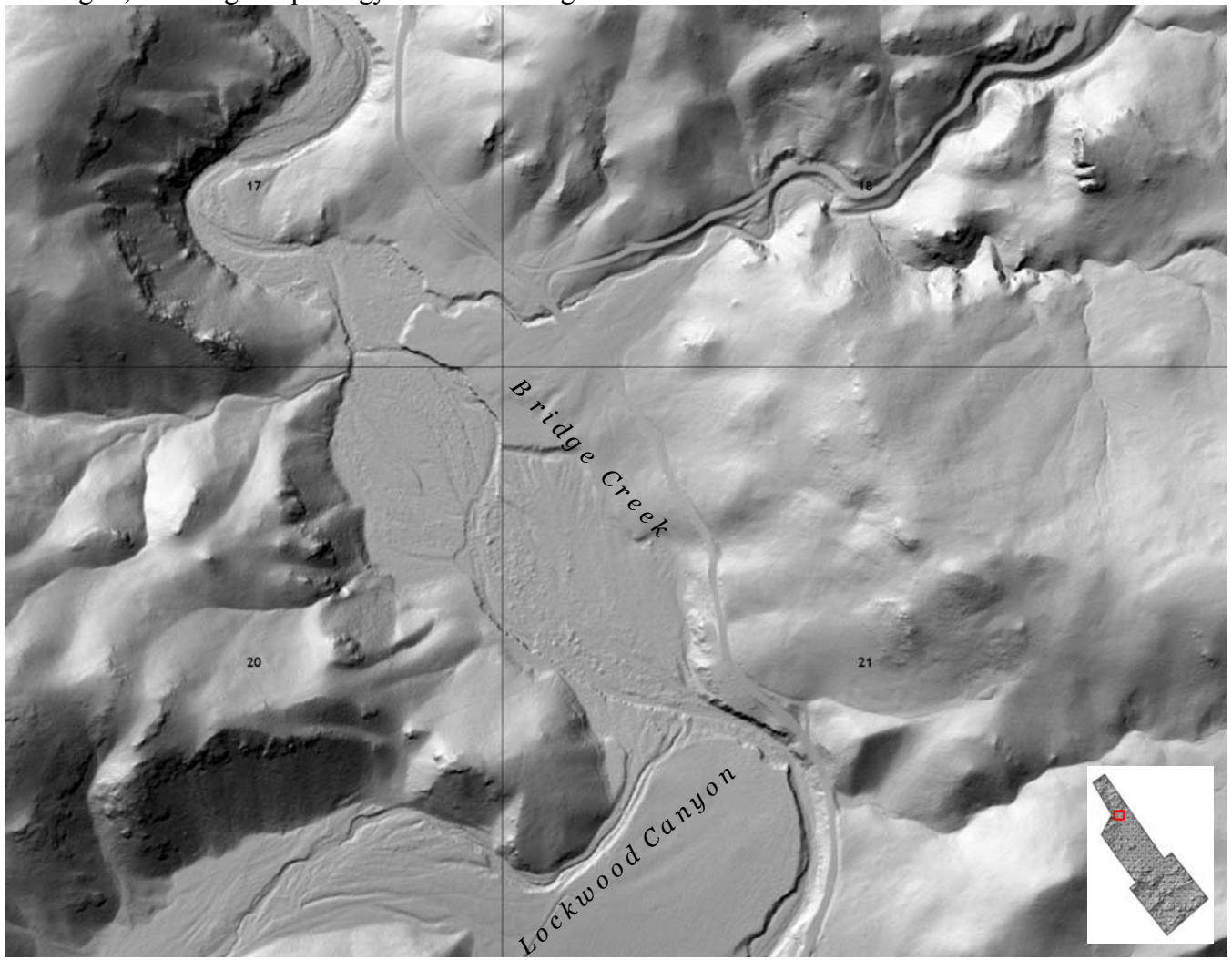

Figure 8. Map of bins 17-18, 20-21, showing Bridge Creek just below Lockwood Canyon. GEOTIFF shown here is derived from all returns with intensity values.

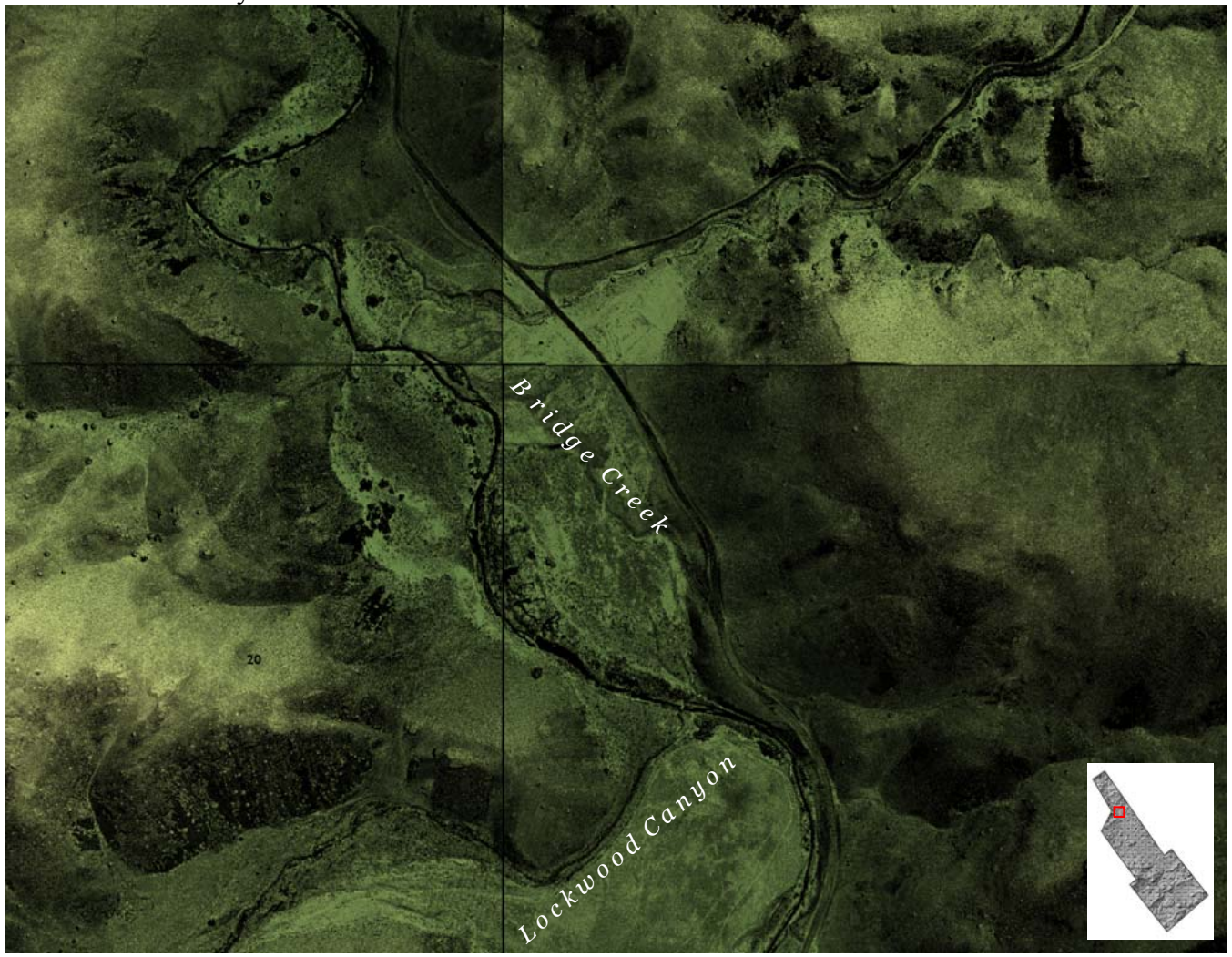

Figure 9. Map of bins 17-18, 20-21, showing Bridge Creek just below Lockwood Canyon. Top image shows 0.5 meter resolution 3-D model derived from bare ground points; bottom image is a point cloud of all returns with intensity values.

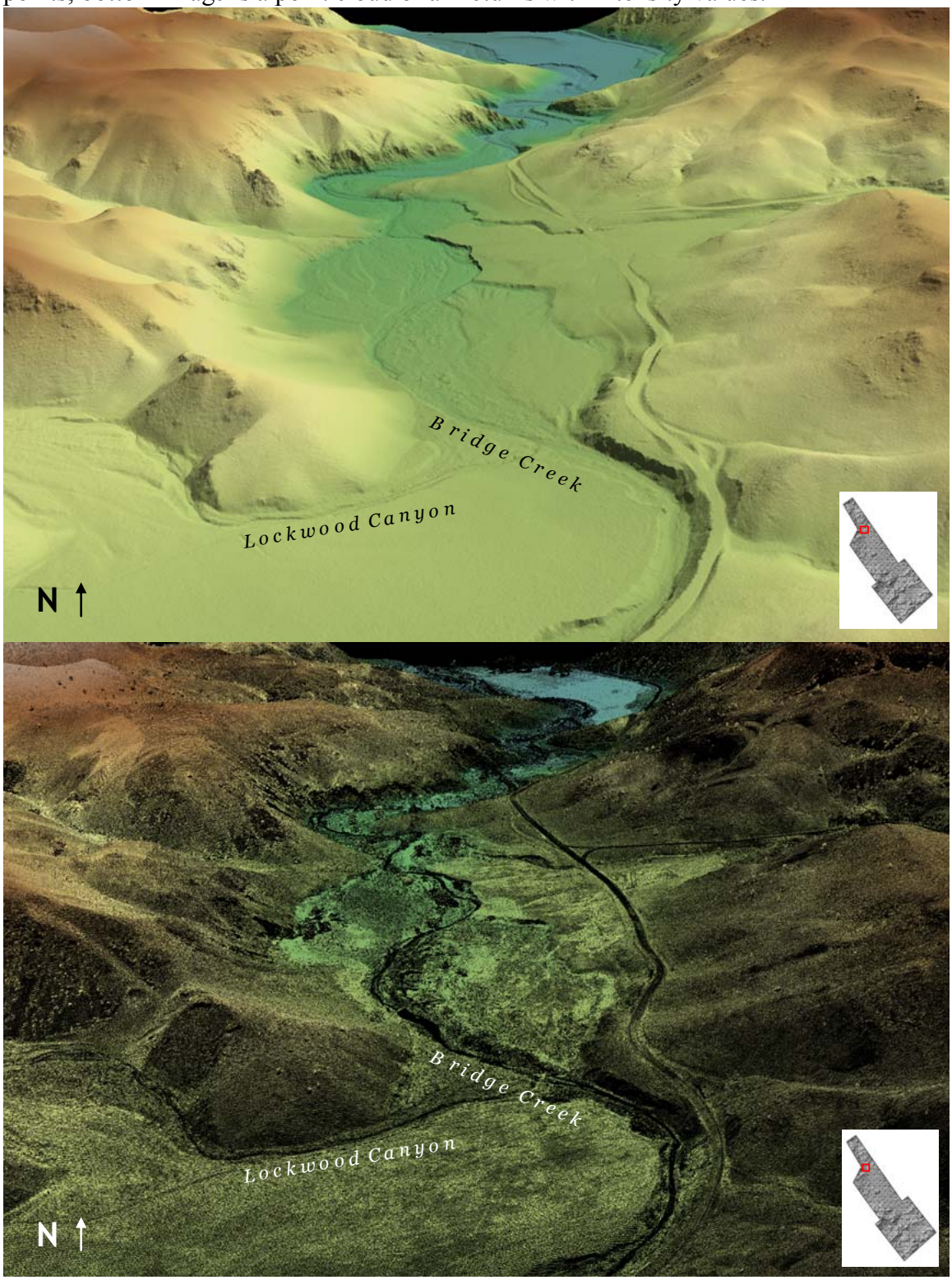

Figure 10. Map of bin 81, showing Bridge Creek below Meyers Canyon. Vegetation grid derived from difference between all returns and bare ground surface, shown over all returns hillshade derived from 1-meter grid. Inset shows location within study area.

Figure 11. Map of bin 81, showing Bridge Creek below Meyers Canyon. Bare ground hillshade, derived from 1-meter grid, showing morphology underneath vegetation.

Figure 12. Map of bin 81, showing Bridge Creek below Meyers Canyon. GEOTIFF shown here is derived from all returns with intensity values.

Figure 13. Map of bin 81, showing Bridge Creek below Meyers Canyon. Top image shows 0.5 meter resolution 3-D model derived from bare ground points; bottom image is a point cloud of all returns with intensity values.

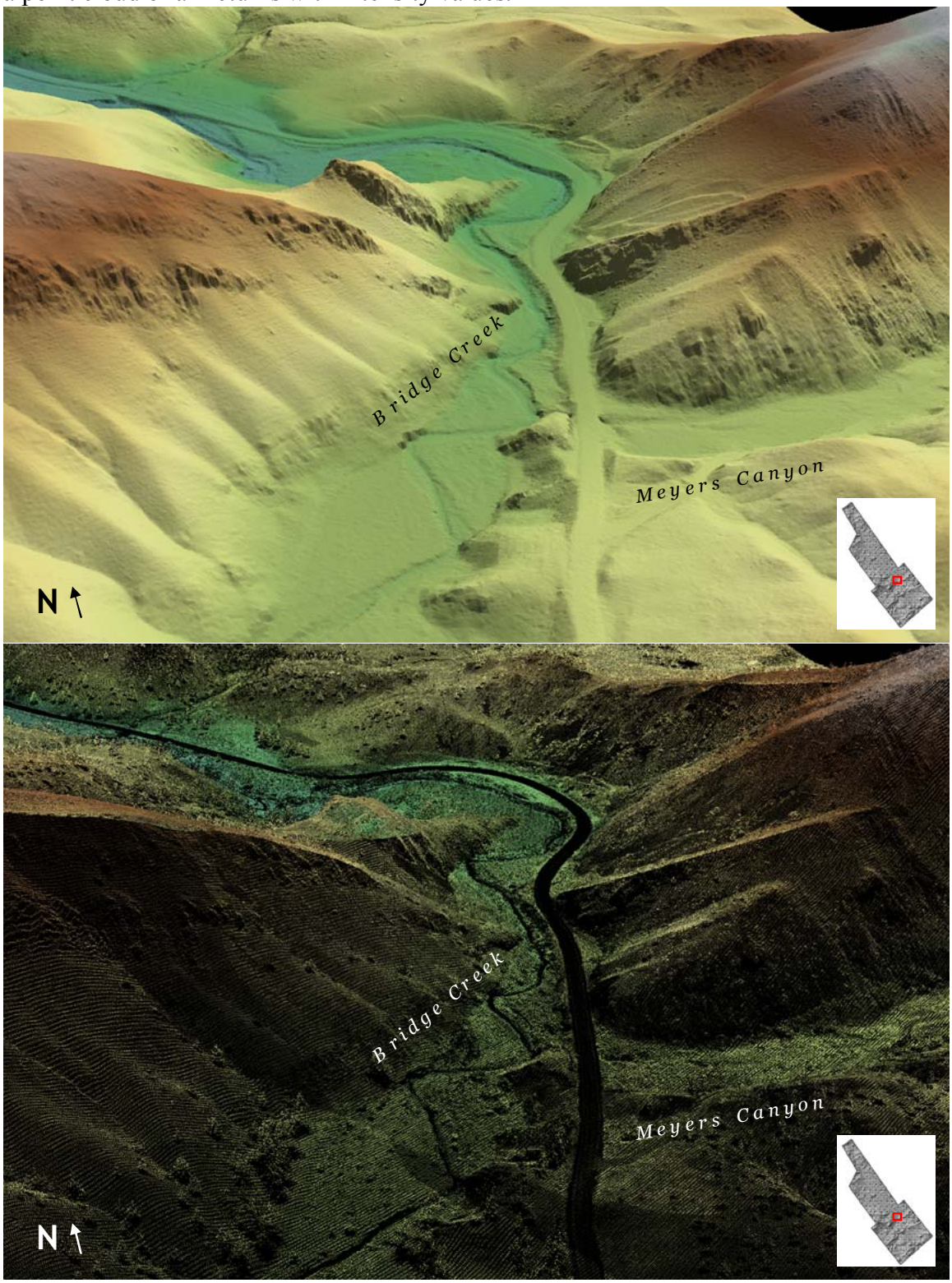

Figure 14. Map of bins 82-83, showing Meyers Canyon. Vegetation grid derived from difference between all returns and bare ground surface, shown over all returns hillshade derived from 1-meter grid. Inset shows location within study area.

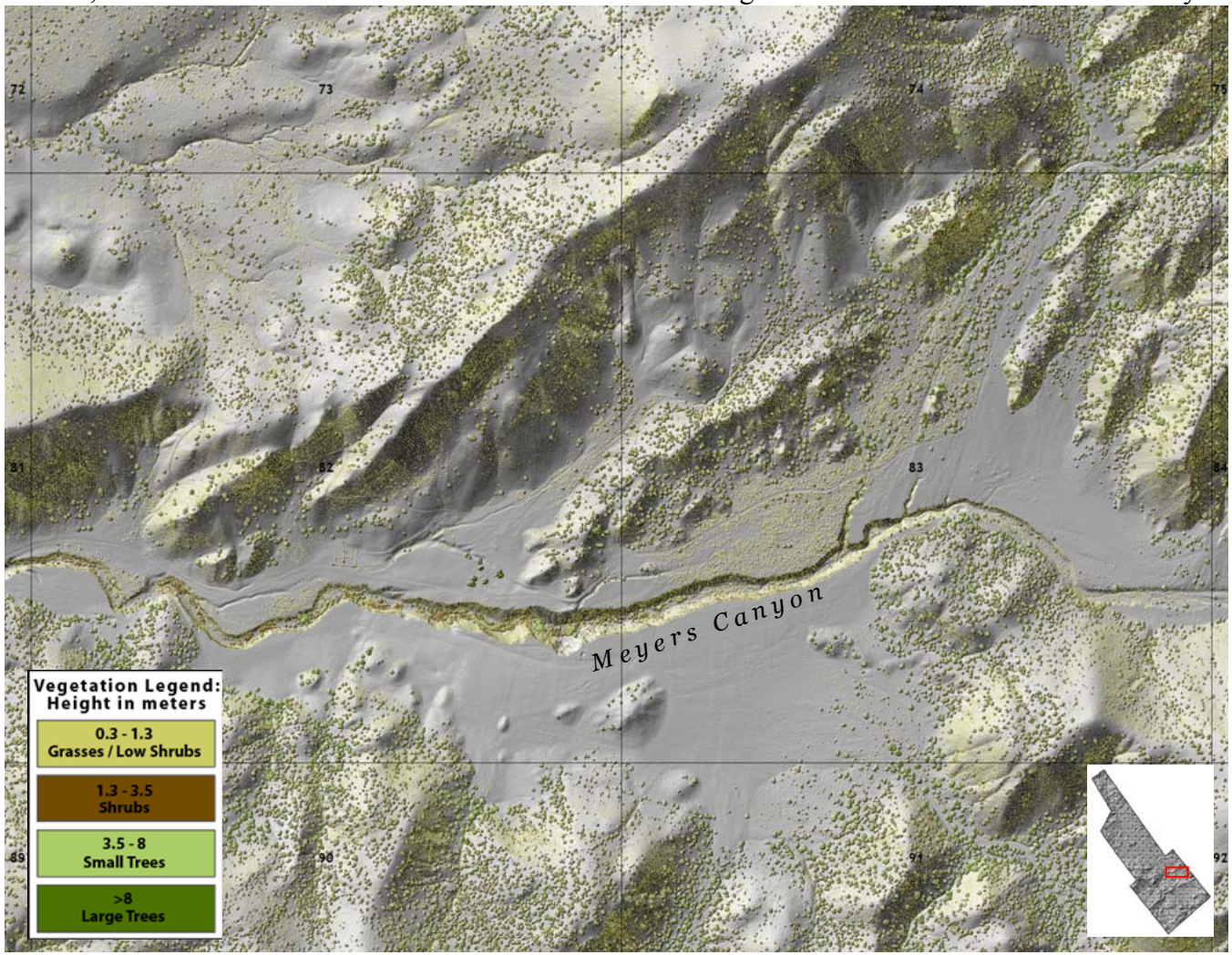

Figure 15. Map of bins 82-83, showing Meyers Canyon. Bare ground hillshade, derived from 1-meter grid, showing morphology underneath vegetation.

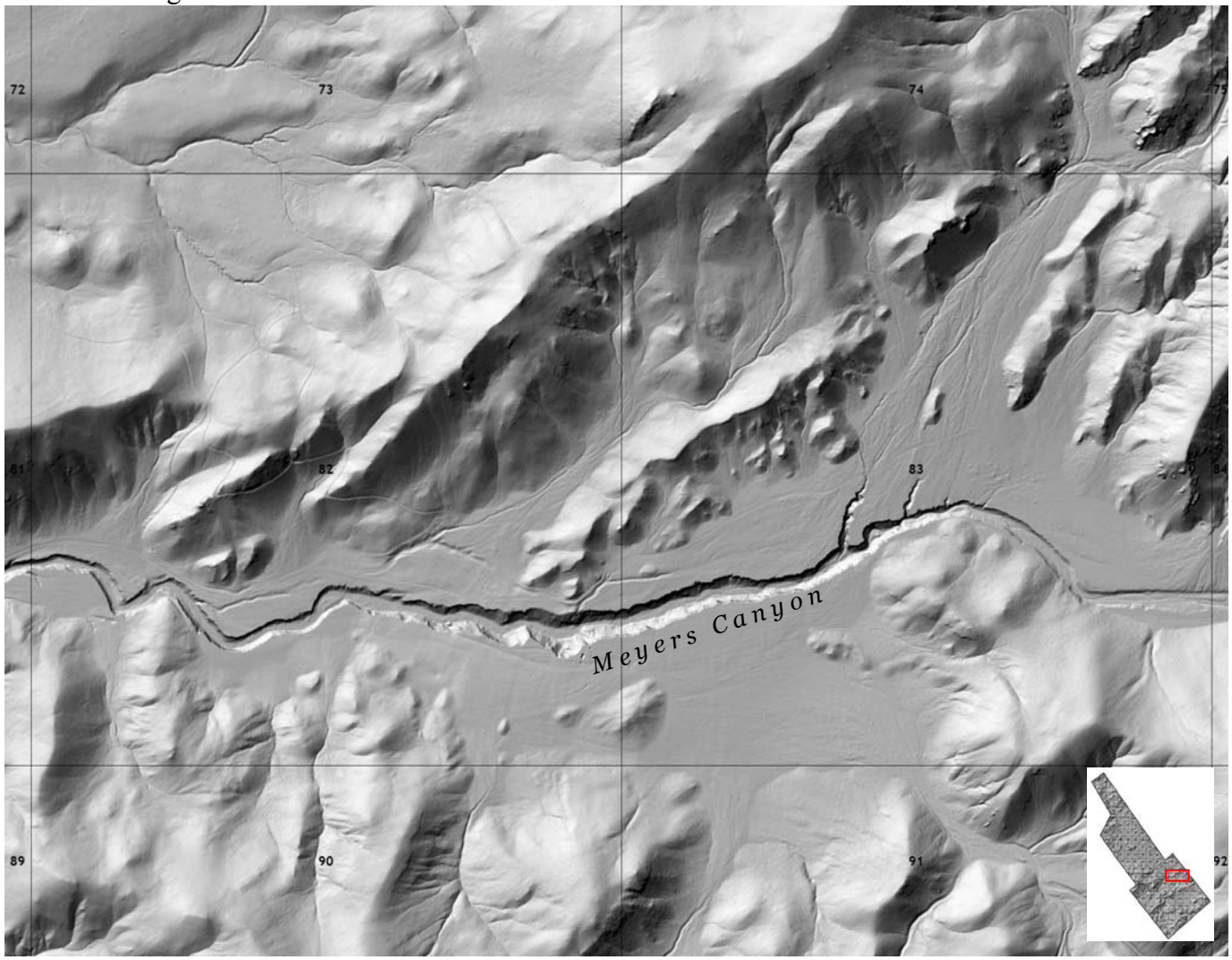

Figure 16. Map of bins 82-83, showing Meyers Canyon. GEOTIFF shown here is derived from all returns with intensity values.

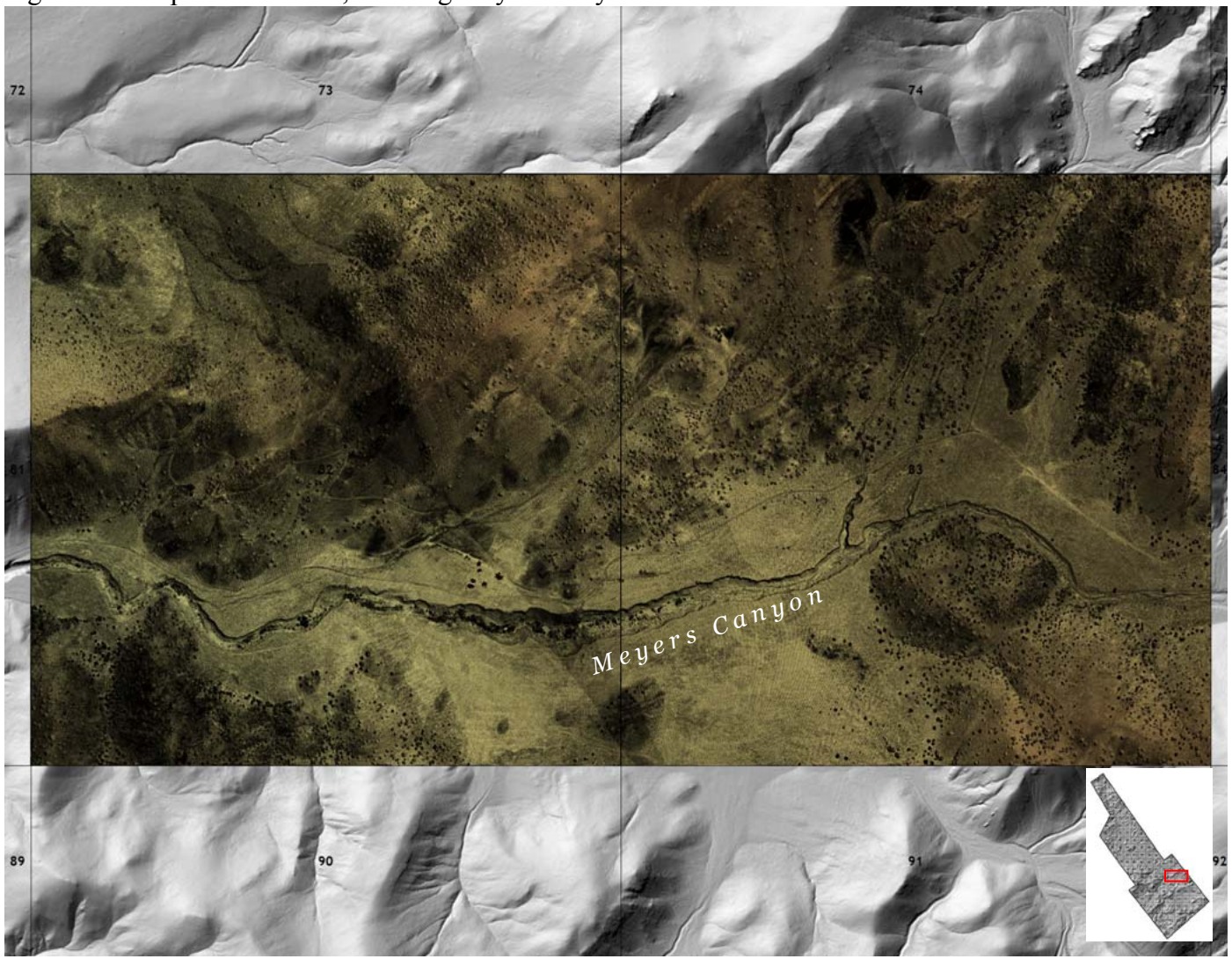

Figure 17. Map of bins 82-83, showing Meyers Canyon. Top image shows 0.5 meter resolution 3-D model derived from bare ground points; bottom image is a point cloud of all returns with intensity values.

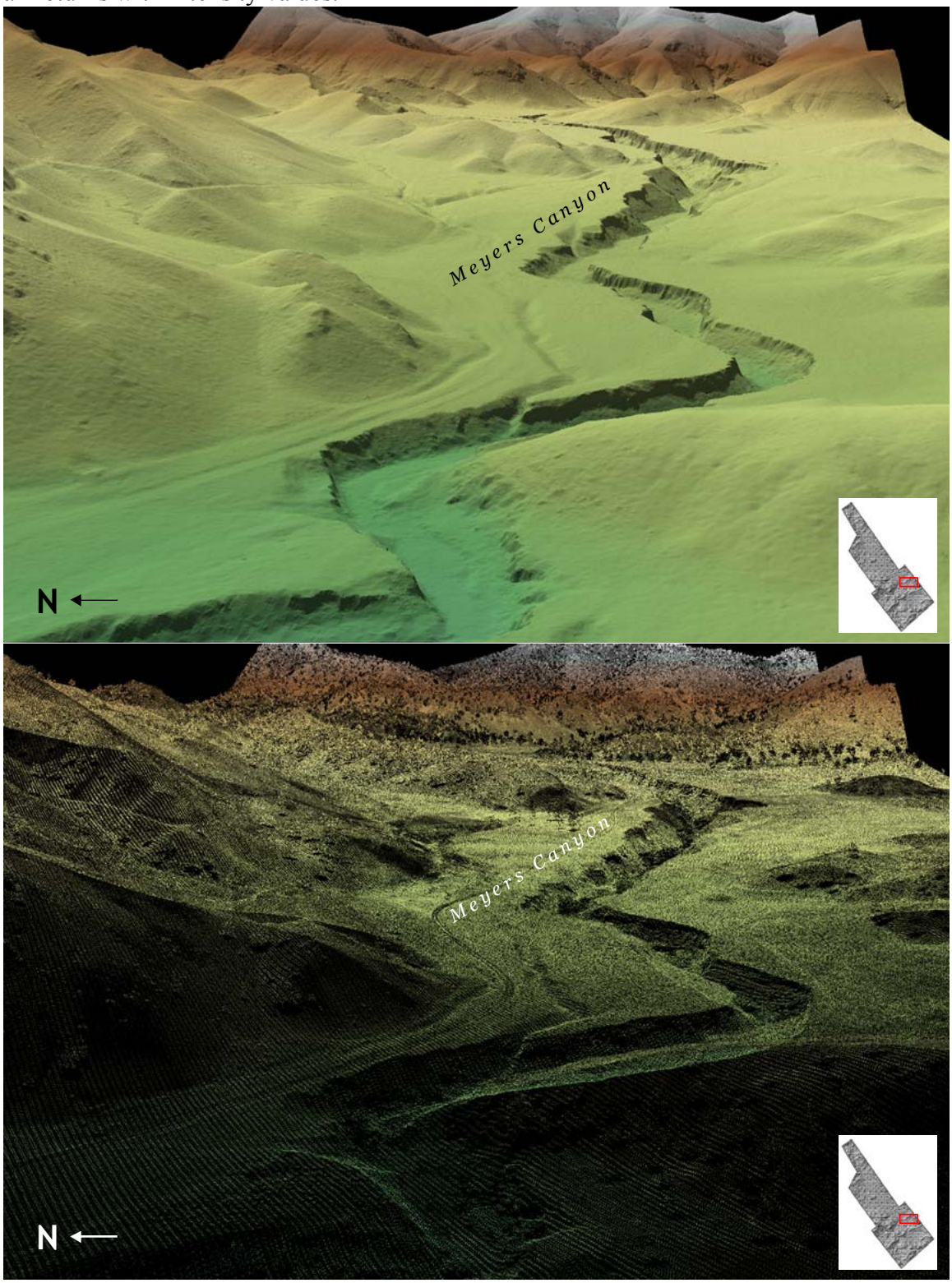

Figure 18. Map of bins 120, showing Bridge Creek downstream of Bailey Butte. Vegetation grid derived from difference between all returns and bare ground surface, shown over all returns hillshade derived from 1-meter grid. Inset shows location within study area.

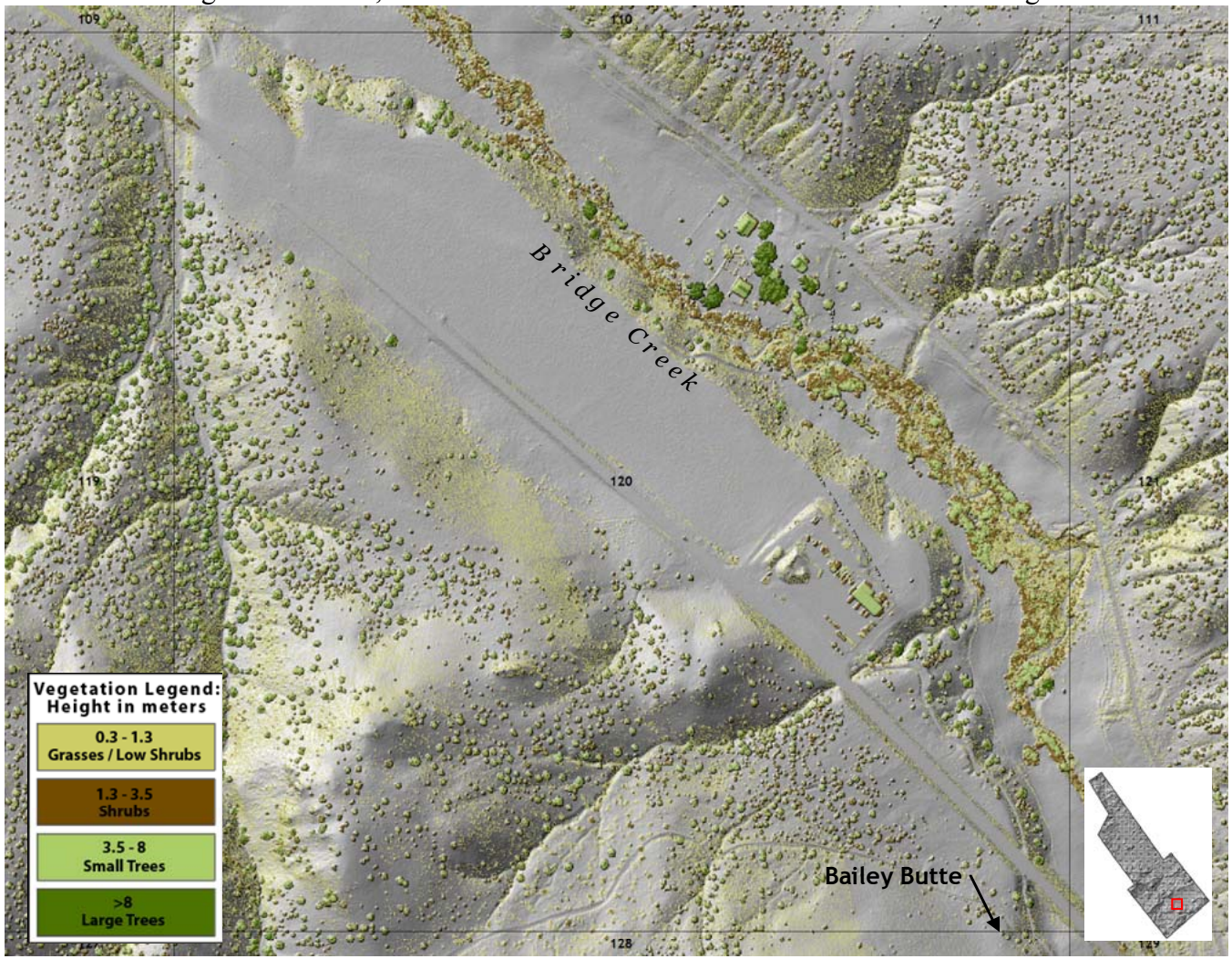

Figure 19. Map of bins 120, showing Bridge Creek downstream of Bailey Butte. Bare ground hillshade, derived from 1-meter grid, showing morphology underneath vegetation.

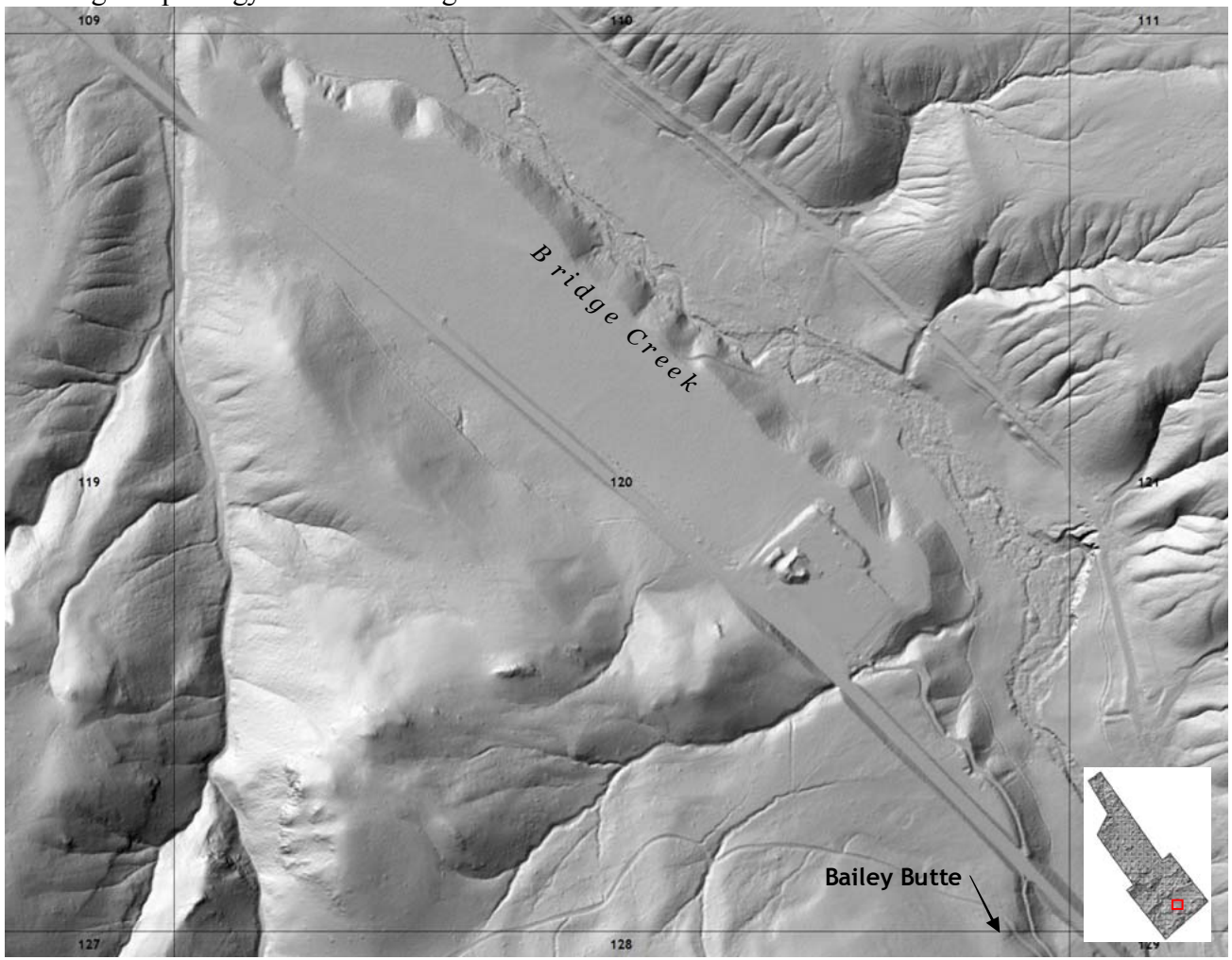

Figure 20. Map of bins 120, showing Bridge Creek downstream of Bailey Butte. GEOTIFF shown here is derived from all returns with intensity values.

Figure 21. Map of bins 120, showing Bridge Creek downstream of Bailey Butte. Top image shows 0.5 meter resolution 3-D model derived from bare ground points; bottom image is a point cloud of all returns with intensity values.